True Egg-shapes

Aysylu Gabdulkhakova[0009−0002−1262−2416],
Jiří Hladůvka[1][0000−0002−5947−8813], and
Walter G. Kropatsch[2][0000−0003−4915−4118]

[1] Comenius University Bratislava, Bratislava, Slovakia
[2] Vienna University of Technology, Vienna, Austria
{aysylu,krw}@prip.tuwien.ac.at

Abstract. A synthetically created discrete ground truth image of an egg-shape could be erroneously assumed as a perfect representation. In fact, it is not suitable for estimating the true egg-shape parameters, such as the minor axis lenght. This paper introduces three algorithms that compute and approximate the true egg-shape parameters. The first is an analytical solution with the disadvantage related to visual interpretation of the input. The second approximates the parameters based on the discrete set of egg-shape points. The third applies the bisection method to achieve high accuracy of the first approach while keeping the intuitiveness of the second. The paper also addresses several computational issues occuring in discrete and digital domains. The main goal is to ensure reliable quantitative evaluation in the complete domain of egg-shapes as well as to improve the accuracy and efficiency of the related applications.

Keywords: egg-shape · multifocal ellipse · Cartesian oval

1 Introduction

The egg-shape is a generalization of the ellipse resembling an oval [5], which makes it a good candidate for approximating a great variety of the real-world objects: from biological cells to tennis rackets [9]. For the shape description, it expresses elongation, orientation, narrowing, but lacks the ground truth. The synthetically generated discrete set of its boundary points is challenging for true parameter estimation [5]. For instance, the points defining the bounding box are not necessarily present. In contrast to ellipse, the egg-shape's minor axis does not pass through the origin. Its length requires the information about the angles that cannot be directly computed from the focal length and major axis length [5].

This paper intends to provide reliable information about the egg-shape for assessing the quality of fitting to oval-shaped objects. The existing approaches either generate the discrete set of egg-shape points [9], or extract them from the level set of the distance field [4], which leads to inaccurate parameter estimates by definition. Since taking the derivatives is not trivial for the egg-shape, this work rests on the newly discovered geometric properties [5], that reflect the exact relations between the egg-shape parts, and the non-gradient based optimization

using the bisection method [3]. The results of this paper provide advantages for shape description and enable to quantitatively evaluate the error upper bounds and, thus, to consciously select the desired accuracy and computational efforts for egg-shape fitting or detection algorithms like [5].

The remainder of this paper is organized as follows. Section 2 overviews the basic terminology related to the egg-shape. Section 3 introduces the three algorithms, while Section 4 compares them in a variety of ways and also covers the digital domain, when the discrete set of egg-shape points is mapped onto the binary image. Section 5 concludes the paper.

2 Terminology

The locus of points that have the same distance to one fixed point is a circle. If the number of fixed points (referred to as focal, or foci) is extended to two, then the locus of points with a constant sum of the distances to them is an ellipse. A further generalization is achieved by adding a positive weight $\mu \in (0, 1]$ to one of the focal points. Except for $\mu = 1$, it results in an oval-shaped higher-order curve [4], called egg-shape.

As opposed to ellipse, the egg-shape has one symmetry axis which passes through F_1 and F_2. For simplicity, let us agree on F_1 to be the origin, i.e. its coordinates are $(0, 0)$, while F_2 is located at $(2f, 0)$. Two egg-shape upper halves are illustrated in Fig. 1 and Fig. 2 as grey filled areas. The *major axis* connects the farthest egg-shape points along the symmetry axis (see $\overline{AB}$ in Fig. 1). The *minor axis* is the longest line segment connecting the egg-shape points which is perpendicular to the major axis (in Fig. 2 the semiminor axis is $\overline{K'K}$). In this regard, let us formalize the egg-shape definition.

Definition 1 (Egg-shape). *Let $F_1 = (0, 0)$ and $F_2 = (2f, 0)$ be the foci with positive weights $w_1 = 1, w_2 = \mu \leq 1$. The points $P = (x, y) \in R^2$ with a constant weighted sum of the distances to F_1 and F_2 form an egg-shape, $\mathsf{ES}(F_1, F_2, \mu; c)$:*

$$\mathsf{ES}(F_1, F_2, \mu; c) = \{P \in \mathbb{R}^2 : \mathsf{d}(P, F_1) + \mu \mathsf{d}(P, F_2) = 2c\} \tag{1a}$$

$$\mathsf{ES}(F_1, F_2, \mu; c) = \{x, y \in \mathbb{R} : \sqrt{x^2 + y^2} + \mu\sqrt{(x - 2f)^2 + y^2} = 2c\}, \tag{1b}$$

where $\mathsf{d}(,)$ denotes the Euclidean distance between the two points.

In particular, (1b) makes it possible to express y:

$$y = \sqrt{\kappa^2 - x^2}, \text{ where } \kappa = \frac{2(c - \mu\sqrt{c^2 + (1 - \mu^2)(f^2 - fx)})}{1 - \mu^2} \tag{2}$$

In the existing literature the egg-shape could be found under a different name: multifocal ellipse [4, 6], generalized conic [4, 8], polyconic [11], multifocal curve [6], polyellipse [11], n-ellipse [13], k-ellipse [12], oval [10], and Cartesian oval [15]. Gabdulkhakova et al. [5] discovered the geometric relations between

$$p = \frac{2(c-\mu f)}{1+\mu} \quad (3) \qquad q = \frac{2\mu f}{1+\mu} \quad (4)$$

$$v = \frac{2f}{1+\mu} \quad (5) \qquad w = \frac{2(c-f)}{1+\mu} \quad (6)$$

$$R = \frac{2c}{1+\mu} \quad (7)$$

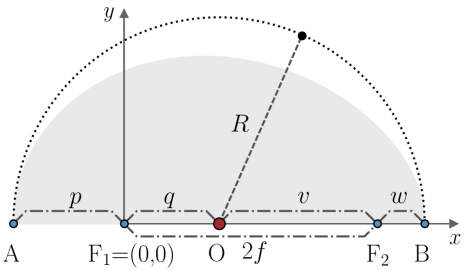


Fig. 1: SEC half (dotted line) and the egg-shape half (grey) which major axis is aligned with x-axis

$$\tau \stackrel{\text{def}}{=} \cos(\beta-\alpha) = \frac{c\cdot\sin\beta}{f} = \frac{2c}{\mu m+n} \quad (8)$$

$$\sin\beta = \sqrt{\frac{1-\tau^2}{1+\mu^2-2\mu\tau}} = \frac{2f-t}{n} \quad (9)$$

$$t = \frac{2\mu m f}{n+\mu m} = \frac{2\mu f(\tau-\mu)}{(1-\mu^2)} \quad (10)$$

$$m = \frac{2c(\tau-\mu)}{\tau(1-\mu^2)} = r\frac{\sqrt{1+\mu^2-2\mu\tau}}{1-\mu\tau} \quad (11)$$

$$k = q - t = \frac{2\mu f(1-\tau)}{1-\mu^2} = \frac{q(1-\tau)}{1-\mu} \quad (12)$$

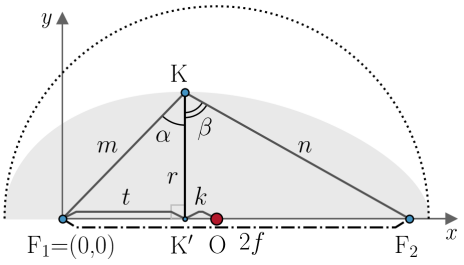


Fig. 2: The distances and angles related to egg-shape y-axis extremum K

Table 1: Egg-shape parameters.

Symbol	Description	Symbol	Description
$F_1 = (0,0)$ $F_2 = (2f,0)$	Focal points	$2f$	Focal length, $\mathsf{d}(F_1,F_2)$
μ	Weight of F_2, $\mu\in(0,1]$. Cosine of the sharp corner half-angle [4]	$2c$	Weighted sum of the distances to F_1 and F_2
A, B	Endpoints of the major axis	$2R$	Major axis length, $\mathsf{d}(A,B)$; SEC diameter
$K = (t,r)$	y-axis extremum of the upper half of the egg-shape	m	Distance from K to F_1
		n	Distance from K to F_2
$K' = (t,0)$	Projection of K onto x-axis; the largest inscribed circle's centre	t	Distance from F_1 to K'
		r	Semiminor axis length; radius of the largest inscribed circle
O	SEC centre	α	$\angle K'KF_1$
k	Distance between the centres of circles: O and K'	β	$\angle K'KF_2$
		τ	$\cos(\beta-\alpha)$

various egg-shape parts. The most valuable of them in the context of the paper are given in (3) - (12) and are followed by Fig. 1 and Fig. 2. The propositions are derived in relation to the smallest enclosing circle (SEC), shown in figures with dotted curve, and to the y-axis extremum of the upper half of the egg-shape, referred to as K. The notations mentioned in this work are collected in Table 1.

3 Finding True Egg-shape Parameters

So far, the true information about the egg-shape was limited to parameters c, f, μ and the discrete set of its points [4, 9]. Thanks to [5], the centres and radii of SEC and the largest inscribed circle can also be used for shape description. This paper proposes methods to compute the above parameters analytically (Alg. 1) or to estimate them from the set of egg-shape points and c, f, μ (Alg. 2–3).

Alg. 1 finds c, f, k and r given R, τ, μ. As can be observed, the egg-shape parameters are tied with the factors expressed by μ and τ. Varying R does not affect the geometrical properties, but the scale. Therefore, it is sufficient to define the pairs of μ and τ that cover the necessary test scenarios.

Algorithm 1: True egg-shape parameters from formulas

Data: Egg-shape parameters: R, τ, μ
Result: Egg-shape parameters: c, f, k, r

1	$c \leftarrow R \cdot (1 + \mu)/2$	- see (7)
2	$\sin\beta \leftarrow \sqrt{(1-\tau^2)}/\sqrt{(1+\mu^2-2\mu\tau)}$	- see (9)
3	$f \leftarrow c \cdot \sin\beta/\tau$	- see (8)
4	$k \leftarrow 2\mu f \cdot (1-\tau)/(1-\mu^2)$	- see (12)
5	$m \leftarrow 2c \cdot (\tau-\mu)/(\tau \cdot (1-\mu^2))$	- see (11)
6	$r \leftarrow m(1-\mu\tau)/\sqrt{1+\mu^2-2\mu\tau}$	- see (11)
7	$t \leftarrow 2\mu f(\tau-\mu)/(1-\mu^2)$	- see (10)

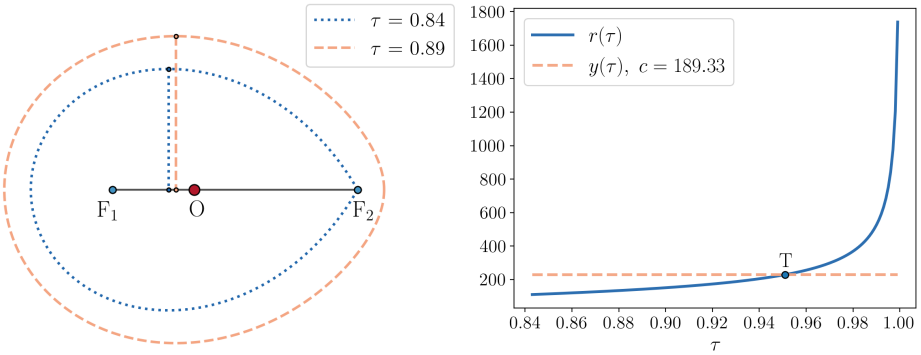
In Alg. 2, $X = \{x_1, .., x_N\}$ and $Y = \{y_1, .., y_N\}$ coordinate pairs could be obtained from (1b) by substituting c, f, μ by specific values and x by $x_i \in X$, where $x_i \in [-p, 2R-p]$, $i \in [1, N]$. Instead, here the polar equation [9] is used. Since the major axis is aligned with x-axis and the origin is at F_1, the foci locations require only the input parameter f (Line 8). Lines 9 and 10 calculate SEC centre and radius. The point with the maximum positive y-value defines K, K' and r (Lines 11-13). In order to find τ (Line 15), it suffices to compute the values of m and n according to their definition: distance from foci to K (Line 14). Finally, Lines 16-17 calculate the values of t and k. As follows from (8) and (9), the ratio c/f can be expressed by μ and τ. Thus, it is valid to fix a particular value of f and vary the factor applied to c, instead of trying all possible pairs of absolute values of f and c.

As follows from (2), taking the derivative of y is not straightforward. To that end, Alg. 3 relies on the bisection method [3] to approximate $K = (t, r)$. Resting

Algorithm 2: Approximate egg-shape parameters from the set of points

Data: Egg-shape parameters: $c,\ f,\ \mu$;
Coordinates of N egg-shape points: $X = \{x_1, .., x_N\},\ Y = \{y_1, .., y_N\}$
Result: Egg-shape parameters: $R,\ k,\ r,\ \tau$

$F_1 \leftarrow [0, 0],\ F_2 \leftarrow [2f, 0]$ - see Tab. 1
$q \leftarrow 2\mu f/(1+\mu),\ O \leftarrow [q, 0]$ - see (4)
$R \leftarrow 2c/(1+\mu)$ - see (7)
$p^* \leftarrow \underset{p\in[1,N]}{\text{argmax}}(Y(p))$
$K \leftarrow [x_{p^*}, y_{p^*}],\ K' \leftarrow [x_{p^*}, 0]$
$r \leftarrow y_{p^*}$
$m \leftarrow \mathsf{d}(K, F_1),\ n \leftarrow \mathsf{d}(K, F_2)$ - see Tab. 1
$\tau \leftarrow 2c/(\mu m + n)$ - see (8)
$t \leftarrow 2\mu m f/(n + \mu m)$ - see (10)
$k \leftarrow q - t$ - see (12)



(a) The confocal egg-shapes for different τ (b) The dependency of r and y on τ

Fig. 3: The results of varying the τ-values while keeping f=112.5 and μ=0.5

on the Bolzano–Cauchy theorem [1], it iteratively finds the root of a continuous function $\mathcal{F}$ defined in an interval $[a, b]$, where $\mathcal{F}(a)$ and $\mathcal{F}(b)$ have the opposite signs. At each step it takes the middle of the interval ($\varsigma = (a+b)/2$) and updates it to $[\varsigma, b]$ or $[a, \varsigma]$ depending on the sign of $\mathcal{F}(\varsigma)$. The process stops, when $\mathcal{F}(\varsigma)$ is sufficiently close to 0. It is guaranteed that the bisection method converges, although, it might be slow, when the initial guess is close to the root [3].

With respect to (1a), fixing the focal points F_1 and F_2 and varying c creates a family of confocal multifocal ellipses [4]. When the τ-value equals the lower limit [5], the egg-shape has a sharp corner at one of the foci. Increasing τ causes the shrinking of k and stretching of r, which results in an egg-shape converging to a circle. Fig. 3 illustrates the above properties. For the fixed f and μ, r grows with an increase of τ (Fig. 3b). When additionally fixing c, i.e. considering the particular egg-shape, it is possible to find t from (10) and then y by substituting

$x = t$ in (2). The resulting function $y(\tau)$ has a limited range of values and intersects $r(\tau)$ at exactly one point - T. The difference between r- and y-values for each τ creates a function, which is negative to the left of T, positive to the right of T and equals 0 at T. So, it is possible to apply the bisection method to find K. Due to numerical precision in the digital domain, it suffices to define the non-strict inequalities, where ε could express the minimum difference between the two floating-point numbers.

Algorithm 3: Bisection method for finding the egg-shape parameters

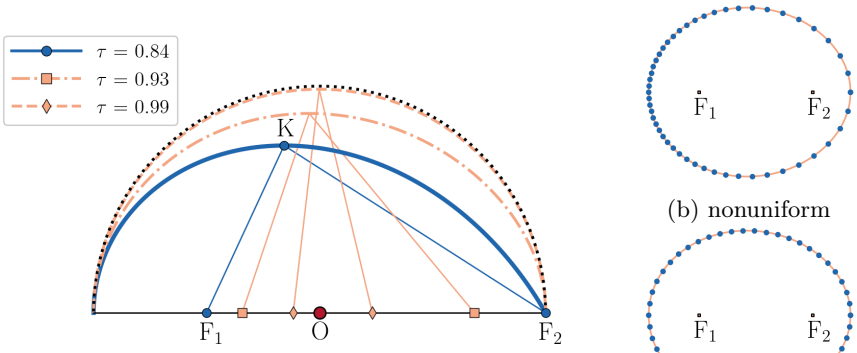
Data: Error threshold: ε; Egg-shape parameters: $c,\ f,\ \mu$
Result: Egg-shape parameters: $k,\ r,\ \tau$

$a \leftarrow (\mu + \sqrt{\mu^2 + 8})/4 \approx (\mu + 1)/2$ - see τ lower limit [5]
$b \leftarrow 1$ - see τ upper limit [5]
while $(b - a) \geq \varepsilon$ **do**
  $\varsigma = (a + b)/2$
  $t \leftarrow 2\mu f(\varsigma - \mu)/(1 - \mu^2)$ - see (10)
  $r \leftarrow t(1 - \mu\varsigma)/\mu\sqrt{1 - \varsigma^2}$ - see (8) – (11)
  $\kappa \leftarrow 2(c - \mu\sqrt{c^2 + (1 - \mu^2)(f^2 - ft)})/(1 - \mu^2)$ - see (2)
  $y \leftarrow \sqrt{\kappa^2 - t^2}$ - see (2)
  if $(r - y) < 0$ **then**
    $a \leftarrow \varsigma$
  else
    $b \leftarrow \varsigma$
  end
end
$k \leftarrow 2\mu f/(1 + \mu) - t$ - see (4) and (12)
$\tau \leftarrow \varsigma$
return $k,\ r,\ \tau$

4 Experimental Results

Alg. 1 relies purely on formulas, thus, its advantage is high accuracy of the parameter computation. This strategy, however, is not intuitive, since relying on angular parameters that are hard for visual interpretation. As an example, observe several egg-shape halves having $\mu = 0.5$ and various values of τ (Fig. 4a). In particular, $\tau = 0.84$ creates the sharp corner, when F_2 coincides with B and $c = f$. Similarly to $\triangle F_1 K F_2$, the remaining triangles are formed by the foci and the highest point of the corresponding egg-shape half. The red circle marks O, which in turn divides the focal distances in the ratio $\mu : 1$ (see (4)–(5)).

In Alg. 2 the boundary sampling properties affect the quality of finding k, r and τ. This issue is not only about the number of points N. Hladůvka et. al [9] distinguish nonuniform (angle-based) and uniform (arc-length-based) samplings,



(a) The egg-shape halves for $\mu = 0.5$ and various τ. Dotted curve shows SEC

(b) nonuniform

(c) uniform

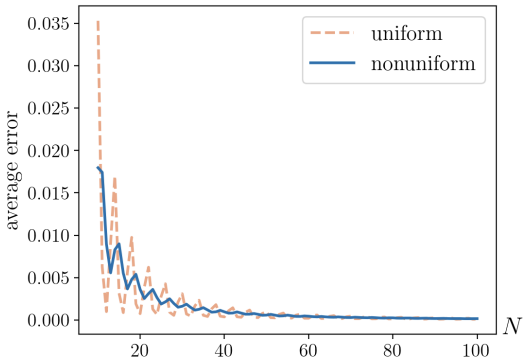
Fig. 4: Three ways to express the egg-shape

shown in Fig. 4b–4c. In any case it is not guaranteed that all the necessary points for estimating robustly the egg-shape parameters are present in the set.

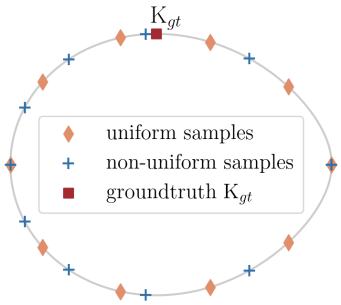
Alg. 3 is the golden mean between the first two methods: it combines the visual intuitiveness of the input parameters with the accuracy limited to the smallest possible difference between the neighboring real values, or $(b-a)$. Since dividing the interval by half in each while loop, it ends up in a logarithmic number of iterations. To evaluate this method, Alg. 1 generated the true parameters for $R_{gt} = 1$ and the unique pairs of values (μ_{gt}, τ_{gt}), where μ_{gt} is in the interval $[0.001, 1]$ with the step 0.001, and τ_{gt} ranges in the interval $[(\mu_{gt}+\sqrt{\mu_{gt}^2+8})/4, 1]$ with the step 0.0001 [5]. For 1533280 combinations of the egg-shape parameters and $\varepsilon = 2.22 \times 10^{-16}$ the maximum number of iterations is 52. In 99% of the cases the error for r is less than 2.04×10^{-14} and for k - less than 1.38×10^{-15}. The remaining cases correspond to almost circular shapes or elongated ellipses.

4.1 Evaluation of Alg. 2

Test Dataset. For this purpose, Alg. 1 computed 302 combinations of the egg-shape parameters for $R_{gt} = 1$. Each of them corresponds to a unique (μ_{gt}, τ_{gt}) pair, where μ_{gt} ranges from 0.05 to 1 with the step 0.05, and τ_{gt} belongs to the interval $[(\mu_{gt} + \sqrt{\mu_{gt}^2+8})/4, 1]$ with the step 0.01 [5]. Then, each combination is used to generate the uniform and nonuniform samplings with $N \in [10, 100]$ points leading to 302×91=27482 discrete sets of points of each type, or 54964 samplings in total. Note, the ground truth dataset contains the egg-shapes enclosed in a unit circle. For an arbitrary R^*, the absolute error values in Section 4.1 should be multiplied by R^* (refer to Sec. 3).



(a) the average difference between r (Alg. 2) and r_{gt} (Alg. 1) in the case of nonuniform and uniform sampling



(b) the egg-shape samplings and the ground truth K_{gt} for $c_{gt} = 22.5$, $f_{gt} = 19,\ \mu_{gt} = 0.5,\ N_{gt} = 10$

Fig. 5: r and r_{gt} for sampled egg-shapes

Approximating K Based on Sampling Type. In Alg. 2 the radius R, the positions of F_1, F_2, and O are expressed with formulas. These parameters can deviate from the true value, due to numerical precision. Finding the location of K as the highest egg-shape point (Line 12) introduces an error, due to sampling. Especially, when N is not large. For example, for various N in $[10, 100]$, Fig. 5a illustrates the average difference between the y-coordinates, i.e. r (Alg. 2) and r_{gt} (Alg. 1), when using nonuniform (solid) and uniform (dashed) samples. Note, in 47% of the test cases the nonuniform sampling lead to a better approximation of r_{gt}. One such example is in Fig. 5b: K_{gt} (square) is closer to the sample from the nonuniform set (plus) than to the sample from the uniform set (rhombus). This figure also shows that the difference between the estimated K and K_{gt} is mainly caused by the x-coordinate. This fact highly impacts t and k, when computed as $\mathsf{d}(F_1, K')$ and $\mathsf{d}(K', O)$ correspondingly (Tab. 1). In Fig. 6b observe the average $|\mathsf{d}(F_1, K') - t_{gt}|$ and $|\mathsf{d}(K', O) - k_{gt}|$ for various N. Alternatively, both t and k can be expressed by input parameters μ, f and the distances m and n with regard to (10) and (12). Although, m and n are calculated as the distances from foci to K (Line 14), they approximate the ground truth values better than $\mathsf{d}(F_1, K')$ (Fig. 6a). As a result, the accuracy of t- and k-estimate is improved (Fig. 6b).

Sampling May Create K' on the Right of O. In Fig. 6b, the error function takes the absolute value of k. There are cases, when, due to sampling, the point K' is located between O and F_2 (Fig. 7). As a result, after applying Alg. 2, k becomes negative. Theoretically, this is not the case (Cor. 1 in [5]). Therefore, mirroring K' with respect to y-axis and taking the absolute k value is a plausible approximate solution to the problem.

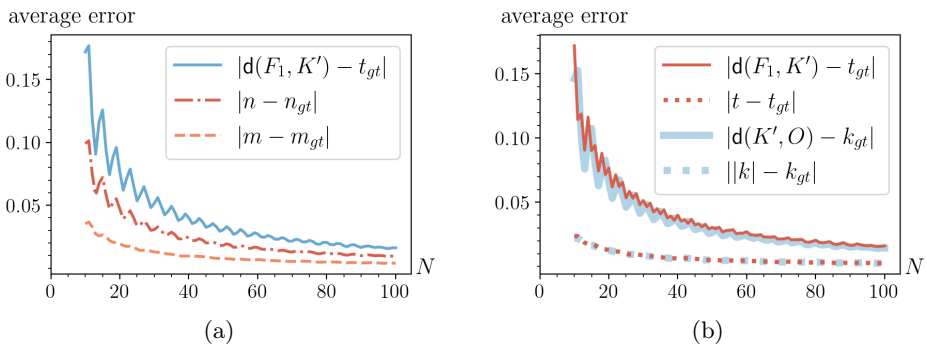


Fig. 6: The errors expressed by the differences between the estimated (Alg. 2) and ground truth (Alg. 1) values averaged for distinct N. Samplings are nonuniform

The negative k appears not often: in 497 ($\approx$ 1.8%) nonuniform and in 228 ($\approx$ 0.8%) uniform samplings from the test dataset. The vast majority of them, 475 ($\approx$ 95%) nonuniform and 226 ($\approx$ 99%) uniform samplings, has the difference to the ground truth less than or equal to 2% of R (or belongs to the interval $[-0.02, 0)$). In general, the increase of N causes the decrease of negative k occurences and values. For uniform samplings, k-values less than -0.001 appear due to a low number of samples, when $N < 40$. When $N \geq 60$, the k-values are above -0.0002, and the related egg-shapes tend to a circle.

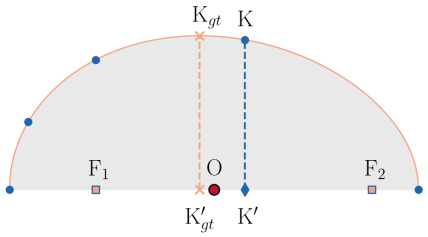


Fig. 7: The example of the nonuniform sampling leading to the negative k value. The ground truth egg-shape parameters: $c_{gt} = 26.25$, $f_{gt} = 20.26$, $\mu_{gt} = 0.75$. The corresponding upper-half egg-shape points (blue circles), $N = 8$.

4.2 Digital image errors

So far the discussion was in the continuous and discrete domains. For classical way to create a digital binary image of the egg-shape, it is sufficient to have a discrete set of its points. Then, the line segments connecting the successive points are rasterized. All the pixels belonging to the rasterized egg-shape boundary or its interior are assigned to 1, whereas the background pixels are 0. As opposed to Alg. 2 and Alg. 3, the parameters like c, f and μ are not available. Thus, despite the presence of critical points A, B and K in the discrete set, estimating R, k and r from the binary image introduces additional errors.

Rasterization. Let the discrete set of egg-shape points cover the digital grid densely, or any two consecutive elements belong to 8-adjacent pixels (vertically, horizontally, or diagonally). The x-, y-coordinates of these points are rounded to the nearest natural number. Then, the maximum rasterization error equals half-length of the pixel diagonal. In case the discrete points are spread in the digital grid sparsely, the rasterization is performed on a polygonal egg-shape approximation. For the proposed scenario, estimating the location of particular points has higher importance than the complete shape. These points define the largest inscribed circle (i.e. K) and SEC (i.e. A, B).

Sampling. If N is even, R equals half-length of the line segment connecting the points corresponding to $0°$ and $180°$. For odd N both points forming the major axis are not necessarily present in the sampling. SEC becomes a circle, which is circumscribed about a triangle containing $0°$-point and a pair of points symmetric with respect to the major axis. In the case of nonuniform sampling, the density of points around $180°$ is higher than around $0°$ [9]. For the same N, it produces smaller R deviation from the ground truth than the uniform sampling.

SEC. Finding SEC given the set of points is a well-studied problem with the classical linear-time solution by Welzl [14]. The error of estimating R and O is bounded by the accuracy of rasterization and sampling.

Largest Inscribed Circle. In order to find k and r, the linear-time algorithm called Distance Transform (DT) [7] is beneficial to use. DT is applied to the complement of the binary image (Sec. 4.2), so, the egg-shape pixels are 0, and the background pixels are 1. DT assigns the distance from every zero-pixel (belonging to the shape) to the nearest nonzero-pixel (background). The coordinates and values of the local maxima in the transformed image correspond to the centres and radii of maximum disks. The coordinates and values of the global maximum relate to the centre (K') and radius (r) of the largest inscribed circle.

DT result depends on the selected metric and method. The exact Euclidean distance [2] enables to avoid extra errors caused by image transformation to some canonical form. It bounds the maximum error of measuring the distance on a digital grid to half-length of the pixel diagonal. On the other side, the radius of the corresponding largest inscribed circle does not necessarily express the latitude of the highest egg-shape point (refer to **Sampling** and **Rasterization**).

5 Conclusion

The paper presents three algorithms to find and approximate the true egg-shape parameters corresponding to the largest inscribed circle, smallest enclosing circle and the cosine of the angle difference at the y-axis extremum. The proposed approaches solve the original problem, that excludes the use of derivatives, at a constant (Alg. 1 and Alg. 2) and logarithmic time (Alg. 3) with the help of

geometric properties and the bisection method. The practical value of this work goes beyond shape description and representation, and could be advantageous in machine learning, optics, analysis of physical deformations, computer-aided design and architecture.

Disclosure of Interests. The authors have no competing interest.

References

1. Bolzano, B.: Rein analytischer Beweis des Lehrsatzes: dass zwischen je zwey Werthen, die ein entgegensetztes Resultat gewaehren, wenigstens eine reelle Wurzel der Gleichung liege, vol. 8. Mayer & Müller (1894)
2. Ciesielski, K.C., Chen, X., Udupa, J.K., Grevera, G.J.: Linear Time Algorithms for Exact Distance Transform. Journal of Mathematical Imaging and Vision **39**(3), 193–209 (2011)
3. Demir, A.: Trisection method by k-Lucas numbers. Applied mathematics and computation **198**(1), 339–345 (2008)
4. Gabdulkhakova, A.: From circles to generalized conics: Enriching the properties of 2D shape representation and description. Tech. Rep. PRIP-TR-156, Pattern Recognition and Image Processing Group, Technische Universität Wien (December 2022)
5. Gabdulkhakova, A.: Geometry-based approach to find the egg-shape parameters. In: Proceedings of the International Conference on Pattern Recognition (ICPR 2026), LNCS. in print (2026)
6. Glaeser, G., Stachel, H., Odehnal, B.: The Universe of Conics: From the Ancient Greeks to 21st Century Developments. Springer Berlin, Heidelberg, 2nd edn. (2016)
7. Gonzalez, R., Woods, R.: Digital Image Processing. Pearson, New York, 4th edn. (2017)
8. Groß, C., Strempel, T.K.: On generalizations of conics and on a generalization of the Fermat-Torricelli problem. The American Mathematical Monthly **105**(8), 732–743 (1998)
9. Hladůvka, J., Kropatsch, W.G.: Fitting egg-shapes to discretized object boundaries. In: Brunetti, S., Frosini, A., Rinaldi, S. (eds.) Discrete Geometry and Mathematical Morphology (DGMM 2024), LNCS, vol. 14605. pp. 107–119. Springer Nature Switzerland, Cham (2024). https://doi.org/10.1007/978-3-031-57793-2_9
10. Maxwell, J.C.: The Scientific Letters and Papers of James Clerk Maxwell: Volume 1, 1846-1862. Cambridge University Press, Cambridge, 1st edn. (1990)
11. Melzak, Z.A., Forsyth, J.S.: Polyconics. I. Polyellipses and optimization. Quarterly of Applied Mathematics **35**(2), 239–255 (1977)
12. Nie, J., Parrilo, P.A., Sturmfels, B.: Semidefinite Representation of the k-Ellipse. In: Algorithms in Algebraic Geometry, The IMA Volumes in Mathematics and its Applications, vol. 146, pp. 117–132. Springer New York, New York (2008)
13. Sekino, J.: n-ellipses and the Minimum Distance Sum Problem. The American Mathematical Monthly **106**(3), 193–202 (1999)
14. Welzl, E.: Smallest enclosing disks (balls and ellipsoids). In: Maurer, H. (ed.) New Results and New Trends in Computer Science, LNCS vol. 555. pp. 359–370. Springer Berlin, Heidelberg (1991). https://doi.org/10.1007/BFb0038202
15. Williamson, B.: The properties of the Cartesian oval treated geometrically. Hermathena **2**(4), 509–518 (1876)